Source Spectra of 2012 Ahar-Varzaghan Double Earthquakes, Northwestern Iran

Meghdad Samaei[1*] and Masakatsu Miyajima[2]

1. Ph.D. Graduate, Kanazawa University, Kanazawa, Japan, * Corresponding Author; email: samaei@stu.kanazawa-u.ac.jp
2. Professor, Kanazawa University, Kanazawa, Japan

Received: 15/04/2015
Accepted: 11/04/2016

ABSTRACT

114 three-component strong motion records from 2012 Ahar-Varzaghan double earthquakes (Mw=6.5, 6.3) are used to study the apparent source spectra of these two events. For this purpose, all the known effects of local site and travel path were deconvolved from the observed spectra. As of path effects (attenuation model), two models are considered: 1) a model developed by the authors in an earlier study with the geometrical spreading form of $R^{-0.9}$ at close distances, 2) a model developed in this study in which the geometrical spreading has the more conventional form of R^{-1} at close distances. These two models have very similar associated Q factors, as the Q factor is more affected by the rate of geometrical spreading at longer distances. It is observed that the inferred source spectrum (particularly Brune stress drop) depends strongly on the considered attenuation model. For the studied events, the apparent observed source spectra for vertical and horizontal components show overall similarity, with horizontal component having bigger scatter and higher fluctuations. The apparent source spectrum of the first event almost perfectly matches the well-known Brune model; whereas the second event is a fair match to the Brune model and is better represented by a double corner frequency model. Out of four double-corner frequency models of source spectra where evaluated here, only the recently developed generalized double-corner-frequency model can successfully reproduce the observed ground motions; the other three lack flexibility in matching the high-frequency spectral level.

Keywords:
Ahar-Varzaghan earthquakes; Source spectra; Brune model; Kappa; Northwestern Iran

1. Introduction

One of the important issues in earthquake hazard assessment is the estimation of the expected ground motion as a function of distance and earthquake magnitude. The ground motion at a particular site is influenced by three main components: source, travel path and local site conditions. Source factors include magnitude, fault geometry, stress drop, rupture process and slip distribution on the fault. Travel path effects include geometrical attenuation, dissipation of seismic energy due to the earth's anelasticity and elastic waves scattering in heterogeneous media. Site factors constitute of a combination of amplification through crustal profile and near-surface diminution. In this study, the first of these three main elements (i.e. source factors) is addressed. Estimation of either of these factors is a step forward in earthquake risk assessment in a region.

In frequency domain, the observed spectrum of ground motion at a site can be separated to contributions from source, travel path and site, each represented by a spectrum. If each of these spectra is estimated well, the combination of them can be used in stochastic simulation/prediction models of strong ground motions like SMSIM [1] or ESXIM [2]. The predicted/simulated strong ground motions are used in seismic design or checking of special

structures at a site [3] or are employed to develop Ground Motion Prediction Equations (GMPEs) to predict maximum amplitudes of ground motions (i.e. PGA, PGV and response spectra) as function of magnitude and distance [4].

The aim of this study is to estimate the apparent source spectra of two strong earthquakes of Ahar-Varzaghan and implications of attenuation models on this estimation. For this purpose, site and travel path effects should be removed from observed spectra. Two models for travel path effects are considered here; the first model is based on an earlier study by the authors [5] and the second model is determined in this study with a different assumption about geometrical spreading compared to the one adopted by Samaei et al. [5]. Moreover, site effects for the strong motion stations are studied to the possible extent and removed from the observed spectra. The remaining spectrum is so called "apparent source spectrum". Comparisons of the estimated spectra with some theoretical and empirical models are also presented.

2. Tectonic Setting

Iran plateau is located in the collision zone of Eurasian plate on one side and Arabian plate on the other side, which caused major crustal shortening and thickening along the Iranian active fold-thrust mountain [6]. In northwestern Iran, the relative motion between these two plates are about 20 mm per year. The deformation in the area near Tabriz is dominated by the North Tabriz Fault, a WNW-ESE trending right-lateral strike-slip fault, which has been responsible for seven historical earthquakes with magnitudes greater than 6 since AD 858 [7].

On August 11, 2012 two destructive earthquakes occurred 11 minutes apart near two towns of Varzaghan and Ahar in Northwestern Iran; the first with moment magnitude of 6.5 at 12:23 UTC and the second with moment magnitude of 6.3 at 12:34 UTC [8], resulting in over 300 deaths and 3000 injuries. These earthquakes have two important aspects: first, they are the biggest events recorded in Northwestern Iran, and second, they are very well recorded events, being recorded on more than 60 strong motion stations on Iran Strong Motion Network (ISMN) out to hypocentral distances of more than 200 km [9], Table (1) and Figure (1). These strong motion accelerograms have provided us with excellent database to study the earthquake parameters in the region.

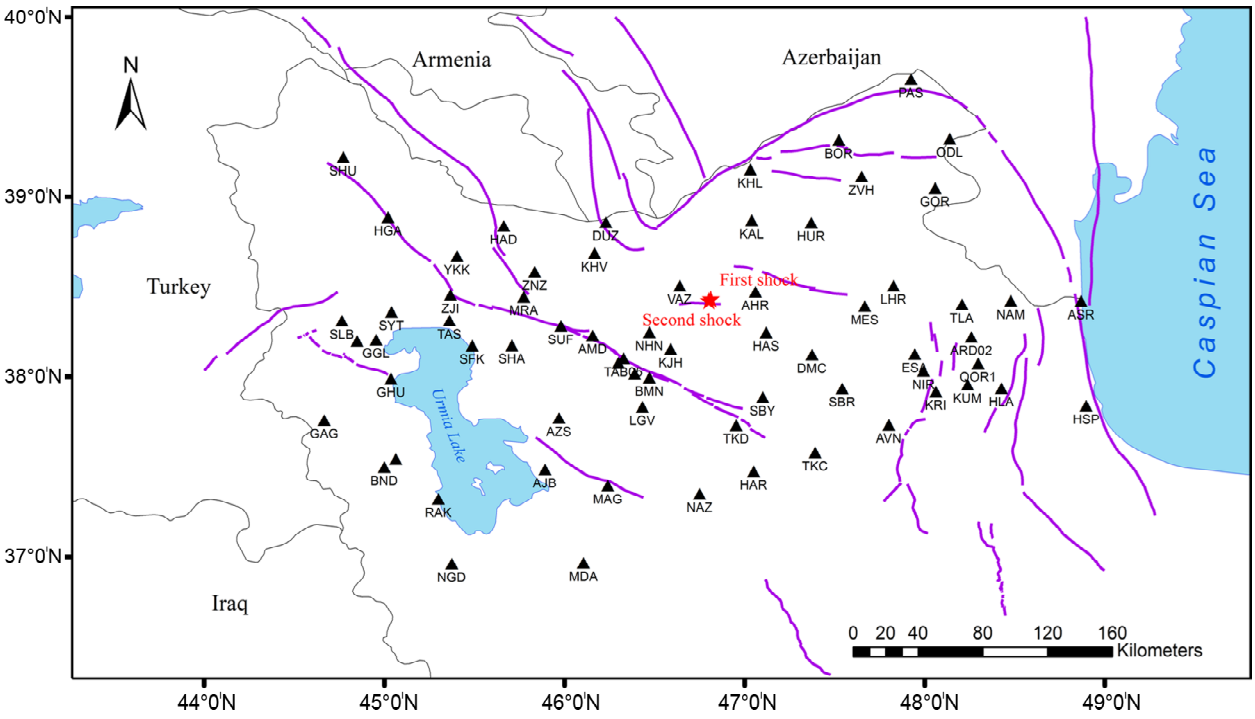

Figure 1. Location of events and stations. Stars denote the location of events and black triangles show the stations.Major faults are also shown as presented by Nazari et al. [10].

Table 1. Earthquakes information.

Event	Date	Time	Latitude	Longitude	Depth (km)	Magnitude	Seismic Moment (N.m)	Reference	No. of Records
First shock	8/11/2012	12:23:15	38.433	46.812	9	Mw 6.5	6.342×10^{18}	IRSC*	49
Second shock	8/11/2012	12:34:35	38.423	46.802	4	Mw 6.3	3.828×10^{18}	IRSC *	65

* Iranian Seismological Center

3. Database

The data used in this study were all recorded by Iran Strong Motion Network (ISMN), which have been installed and maintained by Building and Housing Research Center (BHRC). The BHRC ground-motion database has been expanded continuously during the past decades due to the added new strong-motion stations and occurrence of large earthquakes. So far, more than 10000 strong motion records have been obtained by ISMN since its inception in 1973. By now, this network comprises of 1160 stations composed of three component digital accelerographs in the different active seismic regions of the country [9, 11].

As we noted earlier, Ahar-Varzaghan earthquakes are recorded on more than 60 strong motion stations comprised a database of 114 three-component records. All the stations were equipped with three-component digital SSA2 accelerographs for which the transducer response for them is flat up to 50 Hz. This makes no necessity of correction for instrument response. The sampling rates of the records are 200 Hz (0.005 seconds intervals). Table (1) shows the earthquakes information and Figure (1) shows the location of earthquakes and stations.

Strong motion records of Varzaghan-Ahar double earthquakes are readily available from ISMN website [9].

4. Processing of the Records

Signal processing for the dataset is discussed in detail in Samaei et al. [6], and here is just briefly explained.

After a zero order baseline correction [12], S wave Fourier Amplitude Spectra (FAS) of the acceleration time series were computed using time windows that start with the first arrival of the S wave and end when 90% of the total energy is reached. Time windows were tapered with a 5% cosine taper before calculation of FAS.

Since we work with the data in frequency domain, the most important issue would be the bandwidth that can reliably be used. At high frequencies, FAS starts to fall toward higher frequencies until it flattens and touches the noise floor [13]; the data have been used out to the frequency that FAS touches that floor. This is most recognizable in frequency-FAS plot when frequency is in linear units (not in log units).

The lowest usable frequency is chosen mostly based on the shape of FAS and filtering and inspecting integrated time series. The shape of FAS should be relatively falling toward lower frequencies based on theoretical models of source spectra, and integrated acceleration time series to velocity and displacement should be physically reasonable [14].

Computed FAS for S wave portion of the record is smoothed with a box window of length of five data points and interpolated in 24 logarithmically spaced frequencies between 0.1 to 20 Hz. An example of a record with its raw and interpolated FAS is presented in Figure (2). FAS of the noise in this figure is normalized to the length of the S wave window by multiplying the factor of $(T_u / T_n)^{1/2}$ where T_u and T_n are the durations of the data sample and the noise sample, respectively [15].

5. Method

For obtaining the apparent source spectra, all the known effects to the observed spectra should be removed. Assuming a point source, Fourier spectrum of ground motion consists of contributions of source (E), Path (P) and local site condition (G) [16-17]:

$$Y(f,R) = E(f,M_0)\times P(f,R)\times G(f) \quad (1)$$

where M_0 is the seismic moment and R is the distance from source to observation point.

Source spectrum is parameterized as:

$$E(f,M_0) = CM_0(2\pi f)^2 S(M_0, f) \quad (2)$$

where the constant C is $C = R_{\theta\varphi}FV/(4\pi\rho\beta^3)$, in which $R_{\theta\varphi}$ is the radiation pattern (average value of

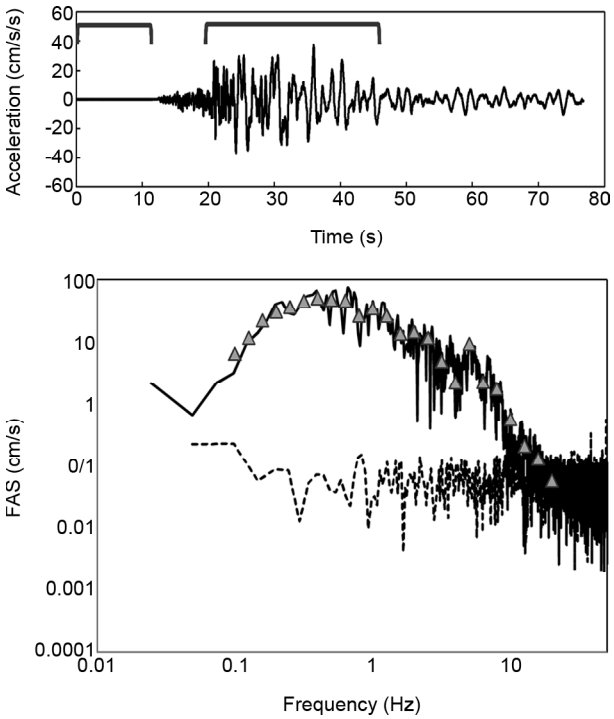

Figure 2. Top: Horizontal T component of the first event, recorded at Basmanj station after zero order baseline correction, with its selected noise and S wave windows (hypocentral distance of 58 km). Bottom: Computed FAS of the S wave (Black line), noise window (dotted line) and smoothed and interpolated FAS of S wave for using in regression and source spectum estimation (triangles).

0.55 for shear waves), F is free-surface amplification (2.0), $V$is the partition onto two horizontal components (0.71), and ρ and β are density and shear-wave velocity in the vicinity of the source [18].

$S(M_0, f)$ is the shape of the displacement source spectrum and can be represented as ω square model of Brune [19-20]:

$$S(f) = \frac{1}{1+(\frac{f}{f_0})^2} \tag{3}$$

where f_0 is the corner frequency, having the following relationship with stress parameter $(\Delta\sigma)$:

$$f_0 = 4.906\times10^6 \beta(\Delta\sigma / M_0)^{1/3} \tag{4}$$

in which f_0 is in Hz, β is in km/s, $\Delta\sigma$ is in bars, and M_0 is in dyn-cm. In the Brune model defined by Eqs. (3) and (4), source spectrum is controlled at low frequencies by seismic moment and at high frequencies by $\Delta\sigma$.

The path effect (P) constitute of multiplication of geometrical spearing (Z) and an elastic attenuation (which includes Q operator):

$$P(f,R) = Z(R)\exp(-\pi f R/Q\beta) \tag{5}$$

These two parameters are estimated for the current database in an earlier study [5]:

$$Z(R) = \begin{cases} \left(\frac{1}{R}\right)^{0.9} & R \le 60km \\ \left(\frac{1}{60}\right)^{0.9}\left(\frac{60}{R}\right)^{0.5} & R > 60km \end{cases} \tag{6}$$

And associated quality factor:

$$Q(f) = 148\, f^{0.62} \tag{7}$$

We call this model "Attenuation model A" hereafter. In this model, geometrical spreading has a gentler slope at close distances (0.9) compared to the typical geometrical spreading (1.0). However, it is shown that the rate of geometrical spreading at close distances is frequency dependent, and as it is explained in Samaei et al. [5], for the frequencies of engineering interest (1 to 10 Hz), the following form of geometrical spreading could be assumed:

$$Z(R) = \begin{cases} \frac{1}{R} & R \le 60km \\ \frac{1}{60}\left(\frac{60}{R}\right)^{0.5} & R > 60km \end{cases} \tag{8}$$

Based on the assumed geometrical spreading, as illustrated in Figure (3), the following function for quality factor is derived:

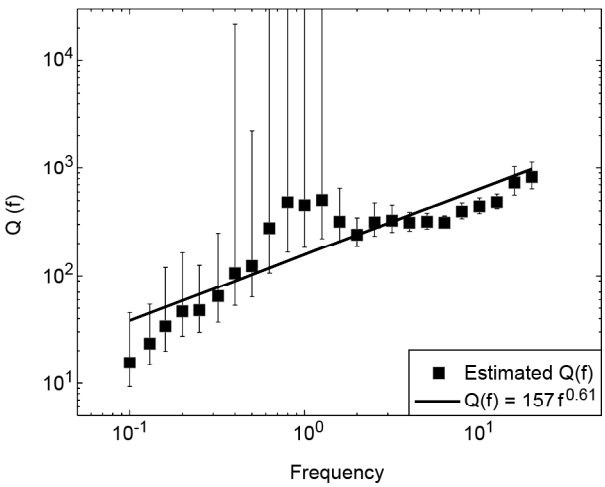

Figure 3. Estimated values for Q(f) with their 90% lower and upper confidence intervals of the coefficient estimates from the regression (blue bars). Solid black line shows the least squares fit to the estimated values.

$$Q(f) = 157\, f^{0.61} \quad (9)$$

The regression method for obtaining this quality factor is as explained in Samaei et al. [5]. The latter attenuation model (Eqs. (8) and (9)) is called "Attenuation model B" hereafter. This way, we are able to evaluate the inferred source spectra in more depth.

It is noticed that although the rate of geometrical spreading is significantly different for two models, this makes little difference to the associated quality factor. This is not surprising as the quality factor majorly affects longer distances where the two models have similar rate of geometrical spreading (0.5).

Finally, site response (G) can be assumed in the form of:

$$G(f) = A(f)\exp(-\pi\kappa_0 f) \quad (10)$$

where $A(f)$ is amplification and κ_0 is the spectral decay parameter at high frequencies for zero distance [13].

High frequency decay parameter at zero distance for current events is estimated by Samaei et al. [21]. In the mentioned sudy, it has been shown that in classical method of estimating kappa, the results are very sensitive to the choices of f_E (where spectrum starts to fall) and f_X (where spectrum reaches the noise floor) and automated procedures for estimating kappa are likely to lead to a biased estimation. Samaei et al. [21] found an obvious concavity in dependency of kappa on distance so the kappa values in distance were regressed to a trilinear shape for which the first line has a zero slope. Based on this trilinear shape, the values of the zero distance kappa are 0.043 and 0.026 for horizontal and vertical components respectively. These results are shown in Figure (4).

It is generally believed that the effect of local site conditions on vertical component of the strong ground motion is negligible [22-24]; therefore, the amplification of unity was assumed for vertical components. For horizontal components, average shear wave velocity to the depth of 30 m (V_{s30}) for some of ISMN stations are available [25]. This includes about half of our recordings. For considering the amplification for horizontal components, available sites were divided into two categories of generic rock (average V_{s30}=620) and generic soil (average V_{s30}=310) sites, and Boore and Joyner [26] crustal amplification factors were used. These factors were originally derived for California based on square root impedance method, but are used extensively in many active tectonic regions around the world. The combined site effects for horizontal components based on Boore and Joyner [26] factors and κ_0 estimated by Samaei et al. [21] are shown in Figure (5).

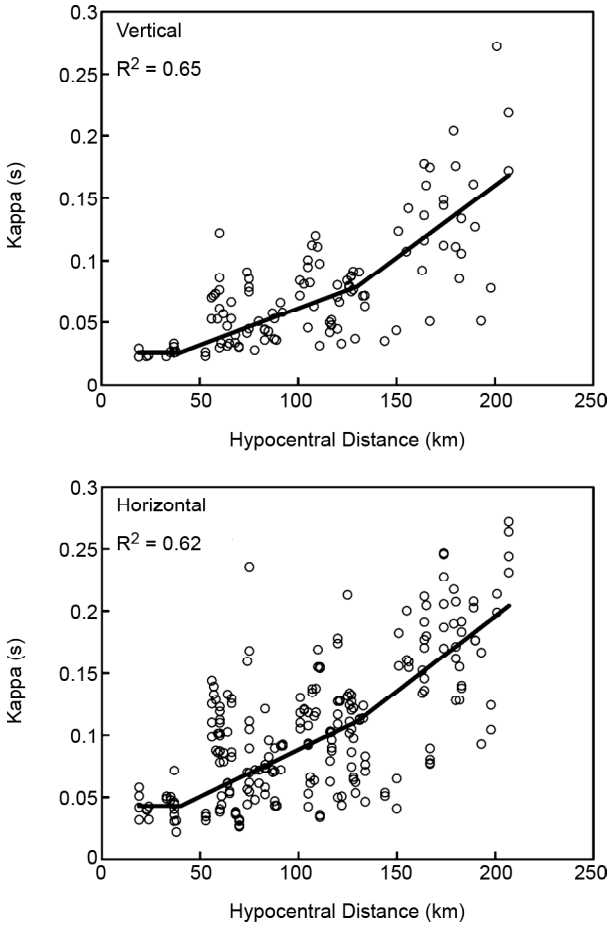

Figure 4. Behavior of kappa in distance for the studied events [21].

7. Results

Known effects of local site and travel path are deconvolved from the observed spectra. This is simply done by playing back the attenuation effects of model A (Eqs. (6) and (7)) or model B (Eqs. (8) and (9)) and site response. Shear wave velocity and density in equation 2 are assumed to be 3.4 km/s and 2.8 g/cm^3 respectively in the region [27].

First, we evaluate the effect of attenuation models on the inferred source spectra from vertical

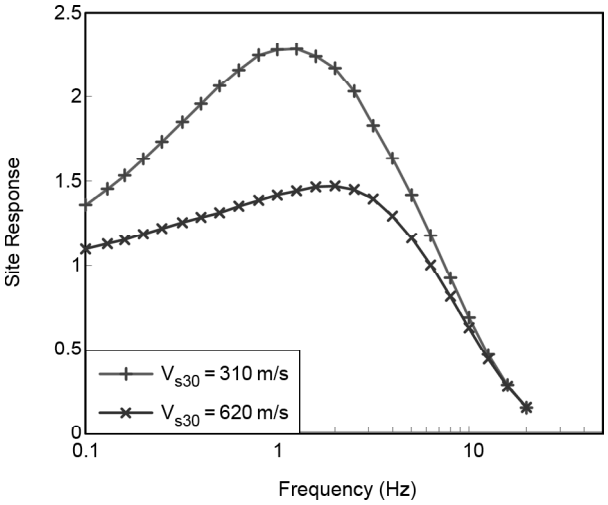

Figure 5. Combined effect of local site for horizontal components, composed of amplification and high frequency diminution. Amplifications at needed frequencies in this study are obtained by interpolation from Boore and Joyner factors, assuming a linear dependency between log frequency and log amplification.

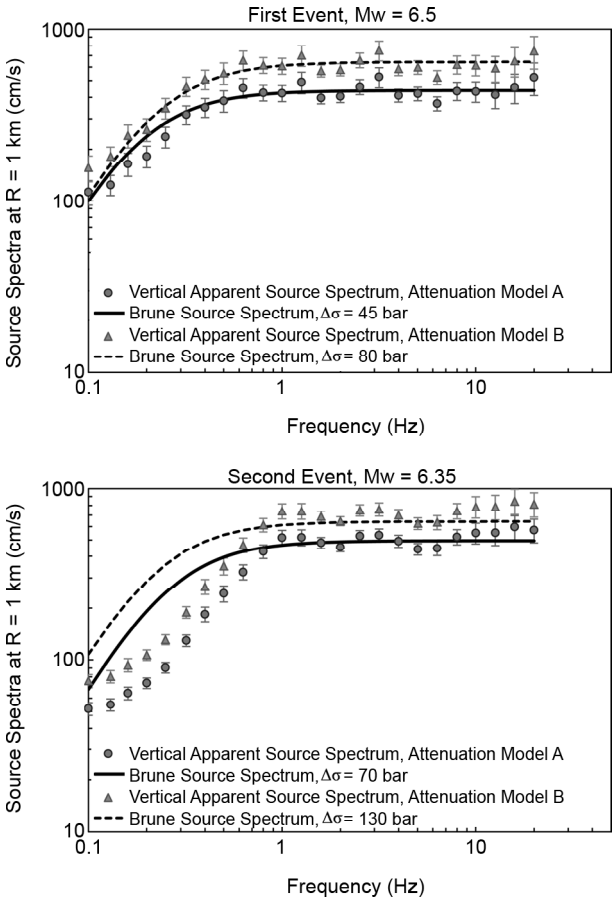

Figure 6. Apparent source spectra at reference distance of 1 km for the studied events for attenuation models A and B. Only observations from vertical component recordings are shown. Error bars are standard error of the source amplitudes, computed from the standard deviation of the mean amplitude, divided by the square root of the number of observations. Small error bars are due to the high number of observations; the standard deviation is in order of 1000 at high frequencies.

component of the recordings. These results are shown in Figure (6) for both events. The source spectra are normalized to the reference distance of 1 km. It is observed that the apparent source spectrum of the first event based on vertical components almost perfectly matches the Brune source model. However, the value of stress drop strongly depends on the attenuation model. The inferred source spectrum from attenuation model A has a value of about 45 bars, whereas for the attenuation model B it is about 80 bars. It is noted that the reported M_0 by IRSC is used as a constraint for matching the Brune source model. Regarding the second event, Brune model is a fair match to the observed data and can predict the high frequency (> 0.8 Hz) level of the spectrum with a stress drop of about 70 bars for Attenuation Model A and 130 bars for Attenuation Model B. The second event seems to be better represented by a two-corner frequency model (e.g. [4, 28]).

The difference between stress parameters inferred from attenuation model A and B is significant. It shows that the stress parameter depends strongly on the attenuation model (geometrical spreading in particular). This is the same conclusion made by Boore et al. [29] and Boore [30]. Therefore, anywhere that determination of stress parameter (Brune stress drop) is of interest, the associated attenuation model should be noted. It is necessary to state that the stress parameter ($\Delta\sigma$) is of fundamental importance in simulations of ground motions, because this parameter along with the seismic moment, largely control the amplitude of high-frequency radiation from the source [30].

Figure (7) further analyzes the source spectra, as it depicts the observation from both vertical and horizontal recordings. Interestingly, there is a similarity of source spectra derived from horizontal and vertical components in a relatively broad frequency band (0.5-20 Hz). In lower frequencies, however, horizontal components systematically show higher amplitudes compared to vertical components. This might be due to the assumed crustal amplification for

horizontal components, as some studies [31-32] show that Boore and Joyner factors underestimate the soil amplification. There is a chance that this under-estimation be more pronounced at low frequencies. This mismatch can also be due to inherent differences in H and V components. In a recent study, Stewart et al. [33] derived GMPEs for vertical components from a global database. They observed complicated (magnitude, distance and period) differences between their derived coefficients and those of their earlier coefficients from horizontal components [34]. These differences are difficult to explain physically. It could be that they are due to some combination of radiation pattern, relative mix of P and S waves, differences in attenuation of P and S waves, refraction due to non-constant crustal velocities, etc. [38].

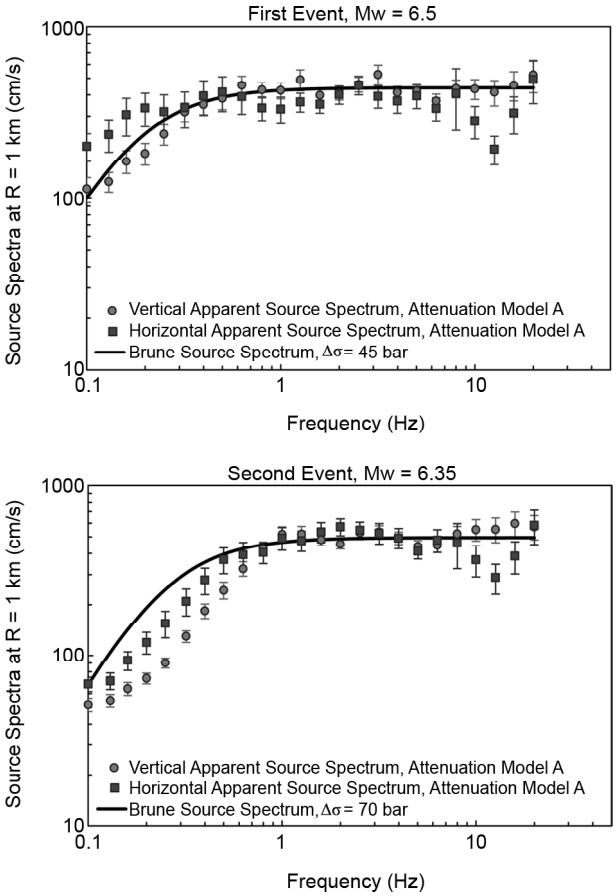

Figure 7. Apparent source spectra at reference distance of 1 km for the studied events for attenuation model A. Error bars are standard error of the source amplitudes, computed from the standard deviation of the mean amplitude, divided by the square root of the number of observations. Small error bars are due to the high number of observations; the standard deviation is in order of 1000 at high frequencies. Corner frequency for the first event is 0.18 and for the second event 0.25 Hz.

Overall, horizontal and vertical spectra are similar with horizontal spectra having higher scatter and higher fluctuations. This is very similar to observations by Chen and Atkinson [35] in which they evaluated source spectra in six different tectonic regions around the world.

The second event is further analyzed here since it shows some signs of following a two-corner frequency source model. Two-corner frequency models are developed to incorporate the complexity near the source due to finite fault effects, and rather than having a single corner frequency of f_0 have two corner frequencies of f_a and f_b.

Table (2) shows the models used in this study. The included models are: first, Atkinson and Boore [4] model developed for earthquakes in Northeastern America; second, Atkinson and Silva [28] model based on California earthquakes; third, Meghdadi and Shoja-Taheri [36] model developed for earthquakes in eastern Iran; and fourth, a generalized double corner frequency model presented in a recent work by Boore et al. [37].

Figure (8) shows the comparison between the observed source spectra and four models of Table (2). The first three models are incapable of reproducing the observed motions. They do a weaker job even comparing with the Brune model. The reason lies in inflexibility of these models. These models do not have a free parameter to match the high-frequency

Table 2. Two corner frequency models of source spectra used in this study.

Model	S(f)	log(f_a)	log(f_b)	log(ε)
Atkinson & Boore 1995	$(1-\varepsilon)/[(1+(f/f_a)^2]+\varepsilon/[1+(f/f_b)^2]$	2.41 - 0.533 **M**	1.43 - 0.188 **M**	2.52 - 0.637 **M**
Atkinson & Silva 2000	$(1-\varepsilon)/[(1+(f/f_a)^2]+\varepsilon/[1+(f/f_b)^2]$	2.181- 0.496 **M**	2.41 - 0.408 **M**	0.605 - 0.255 **M**
Meghdadi & Shoja-Taheri 2014	$1/\{[1+(f/f_a)^2]^{\varepsilon}/[1+(f/f_b)^2]^{1-\varepsilon}\}$	2.69 – 0.56 **M**	3.40 – 0.53 **M**	0.10 – 0.03 **M**
GADCF*	$(1-\varepsilon)/[(1+(f/f_a)^{pf_a}]^{pd_a}+\varepsilon/[1+(f/f_b)^{pf_b}]^{pd_b}$	-	-	-

* Generalized Additive Double Corner Frequency

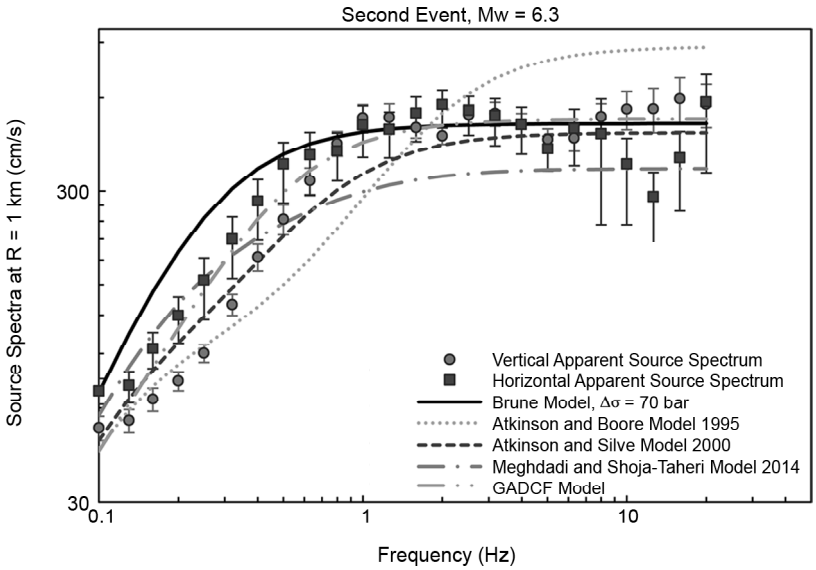

Figure 8. Comparing the second event with some two corner frequency models.

level of the spectra. This is the reason for introducing general double corner frequency models. Two generalized models are introduced by Boore et al. [37], first the multiplicative model and second the additive model. The latter model is discussed here. The generalized additive double-corner-frequency (GADCF) model of the source spectra has the following general form:

$$S(f) = \frac{(1-\varepsilon)}{[(1+(f/f_a)^{pf_a}]^{pd_a}} + \frac{\varepsilon}{[(1+(f/f_b)^{pf_b}]^{pd_b}} \quad (11)$$

where pf and pd stand for power of frequency and power of denominator, and ε is a weighting parameter giving the relative contributions of the two single-corner-frequency spectra. For a flat high-frequency acceleration spectrum, the following constraint must be satisfied:

$$pf_a \times pd_a = pf_b \times pd_b = 1 \quad (12)$$

With this constraint, high frequency level of double corner frequency model can be equal to high frequency level of equivalent single corner frequency model if the following equation is fulfilled:

$$f_b = f_a \sqrt{\frac{(f_0/f_a)^2 - (1-\varepsilon)}{\varepsilon}} \quad (13)$$

where f_0 is the corner frequency of single corner frequency model (e.g. Brune model). This would let the GADCF model at high frequencies be defined by $\Delta\sigma$ as the Brune model.

The GADCF model is fit to the observed apparent source spectra of the second event based on a grid search flowing Eq. (11) and assuming $pf_a = pf_b = 2$ and $pd_a = pd_b = 1$. The result is shown in Figure (8). As it is expected, GADCF model has the same high frequency flat level of the Brune model and matches the observed spectra considerably better than all other models. This indicates on the importance of the flexibility of GADCF model.

8. Conclusions

Source spectra of 2012 Varzaghan-Ahar double earthquakes were evaluated in this study. This was done by deconvolving all the known effects of local site and travel path from the observed spectra. Two attenuation models were considered and it was shown that the inferred source spectra (particularly Brune stress drop) depend strongly on the considered attenuation model (especially geometrical spreading).

Apparent observed source spectra for vertical and horizontal components show overall similarity, with horizontal component showing bigger scatter and higher fluctuations. The apparent source spectra of the first event almost perfectly matches the well-known Brune model; whereas the second event is better represented by a double corner frequency model. Out of four double corner frequency models of source spectra evaluated here, only the recently

developed generalized double-corner-frequency model can successfully reproduce the observed ground motion.

In the present study, source spectra were evaluated using two moderate well-recorded events. For these events, estimated stress parameter of the Brune model ($\Delta\sigma$), depending of the considered attenuation model, ranges between 45 to 130 bars. If a typical geometrical spreading at close distances ($1/R$) is to be considered, the estimated stress drop averages to about 100 bars, which is a typical value that is presented for many active regions around the world.

Acknowledgments

Written communication with David Boore is highly appreciated, from signal processing to interpretation of the results. Furthermore, we thank Azad Yazdani for his valuable comments. Two anonymous reviewers also provided useful remarks and corrections that helped improve the manuscript. We also thank Building and Housing Research Center (BHRC) for providing us with the data, especially Esmaeil Farzanegan who answered our many questions about the stations.

References

1. Boore, D.M. (2005) SMSIM---Fortran programs for simulating ground motions from earthquakes: Version 2.3---A Revision of OFR 96-80-A. US Geological Survey open-file report, 59.

2. Motazedian, D. and Atkinson, G.M. (2005) Stochastic finite-fault modeling based on a dynamic corner frequency. *Bulletin of the Seismological Society of America*, **95**(3), 995-1010.

3. Samaei, M., Miyajima, M., Saffari, H., and Tsurugi, M. (2012) Finite fault modeling of future large earthquake from north Tehran fault in Karaj, Iran. *Journal of Japan Society of Civil Engineers*, Ser A1 (Structural Engineering & Earthquake Engineering (SE/EE)) **68**(4), I_20-I_30.

4. Atkinson, G.M. and Boore, D.M. (1995) Ground-motion relations for eastern North America. *Bulletin of the Seismological Society of America*, **85**(1), 17-30.

5. Samaei, M., Miyajima, M., and Nojima, N. (2016) Attenuation of fourier spectra for 2012 Ahar-Varzaghan double earthquakes, Northwestern Iran. *Journal of the Earth and Space Physics*, **41**(4), 23-38.

6. Berberian, M. (1981) *Active Faulting and Tectonics of Iran*. Geodynamics Series 3.

7. Moradi, A.S., Hatzfeld, D., and Tatar, M. (2011) Microseismicity and seismotectonics of the North Tabriz fault (Iran). *Tectonophysics*, **506**, 22-30.

8. Iranian Seismological Center (IRSC), homepage: http://irsc.ut.ac.ir/

9. Iran Strong Motion Network(ISMN), homepage: www.bhrc.ac.ir/Portal/ISMN

10. Nazari, H., Talebian, M., and Ghorashi, M. (2013). *Seismotectonic Map of NW Iran*. Geological Survey of Iran.

11. Mirzaei Alavijeh, H., Sinaiean, F., Farzanegan, E., and Sadeghi Alavijeh, M. (2007) Iran Strong Motion Network (ISMN) prospects and acheivments. *Procs. of the 5th International Conference on Seismology and Earthquake Engineering*, Tehran, Iran.

12. Boore, D.M. (1999) *Effect of Baseline Corrections on Response Spectra for Two Recordings of the 1999 Chi-Chi, Taiwan Earthquake*. Geological Survey, Open-File Report, 37.

13. Anderson, J.G. and Hough, S.E. (1984) A model for the shape of the Fourier amplitude spectrum of acceleration at high frequencies. *Bulletin of the Seismological Society of America*, **74**, 1969-1993.

14. Boore, D.M. and Bommer, J.J. (2005) Processing of strong-motion accelerograms: needs, options and consequences. *Soil Dynamics and Earthquake Engineering*, **25**, 93-115.

15. Boatwright, J., Fletcher, J.B., and Fumal, T.E. (1991) A general inversion scheme for source, site, and propagation characteristics using multiply recorded sets of moderate-size earthquakes. *Bulletin of the Seismological Society of America*, **81**, 1754-1782.

16. Boore, D.M. (1983) Stochastic simulation of high-frequency ground motions based on seismological models of the radiated spectra. *Bulletin of the Seismological Society of America*, **73**, 1865-1894.

17. Boore, D.M. (2003) Simulation of ground motion using the stochastic method. *Pure and Applied Geophysics*, **160**, 635-676.

18. Atkinson, G.M. and Boore, D.M. (2014) The attenuation of Fourier amplitudes for rock sites in eastern north America. *Bulletin of the Seismological Society of America*, **104**, 513-528.

19. Brune, J.N. (1970) Tectonic stress and the spectra of seismic shear waves from earthquakes. *Journal of Geophysical Research*, **75**, 4997-5009.

20. Brune, J.N. (1971) Tectonic stress and the spectra of seismic shear waves from earthquakes: correction. *Journal of Geophysical Research*, **76**, 5002.

21. Samaei, M., Miyajima, M., Yazdani, A., and Jaafari, F. (2016) High frequency decay parameter (kappa) for Ahar-Varzaghan double earthquakes, Iran (Mw 6.5 & 6.3). *Journal of Earthquake and Tsunami*, **10**(2).

22. Lermo, J., and Chavez-Garcia, F.J. (1993) Site effect evaluation using spectral ratios with only one station. *Bulletin of the Seismological Society of America*, **83**, 1574-1594.

23. Siddiqqi, J., and Atkinson, G.M. (2002) Ground-motion amplification at rock sites across Canada as determined from the horizontal-to-vertical component ratio. *Bulletin of the Seismological Society of America*, **92**, 877-884.

24. Atkinson, G.M. (2004) Empirical attenuation of ground-motion spectral amplitudes in southeastern Canada and the northeastern United States. *Bulletin of the Seismological Society of America*, **94**, 1079-1095.

25. Sinaeian, F., Mirzaei Alavijeh, H., and Farzanegan, E. (2010) *Site Geology Investigation in Accelerometric Stations Using Seismic Refraction Method in Ardebil and East Azarbayejan Provinces. Vol. 2, 50 stations, Center of Iran, Tehran, Iran*. BHRC Publication No R-532, Building and Housing Research, (In Persian).

26. Boore, D.M. and Joyner, W.B. (1997) Site amplifications for generic rock sites. *Bulletin of the Seismological Society of America*, **87**, 327-341.

27. Taghizadeh-Farahmand, F., Sodoudi, F., Afsari, N., and Ghassemi, M.R. (2010) Lithospheric structure of NW Iran from P and S receiver functions. *Journal of Seismology*, **14**, 823-836.

28. Atkinson, G.M., and Silva, W. (2000) Stochastic modeling of California ground motions. *Bulletin of the Seismological Society of America*, **90**, 255-274.

29. Boore, D.M., Campbell, K.W., and Atkinson, G.M. (2010) Determination of stress parameters for eight well-recorded earthquakes in eastern North America. *Bulletin of the Seismological Society of America*, **100**, 1632-1645.

30. Boore, D.M. (2012) Updated determination of stress parameters for nine well-recorded earthquakes in eastern North America. *Seismological Research Letters*, **83**, 190-199.

31. Poggi, V., Edwards, B., and Fah, D. (2011) Derivation of a reference shear-wave velocity model from empirical site amplification. *Bulletin of the Seismological Society of America*, **101**, 258-274.

32. Boore, D.M. (2013) The uses and limitations of the square root impedance method for computing site amplification. *Bulletin of the Seismological Society of America*, **103**, 2356-2368.

33. Stewart, J.P., Boore, D.M., Seyhan, E., and Atkinson, G.M. (2015) NGA-West2 equations for predicting vertical-component PGA, PGV, and 5%-damped PSA from shallow crustal earthquakes. *Earthquake Spectra*, **30**, 1057-1085.

34. Boore, D.M., Stewart, J.P., Seyhan, E., and Atkinson, G.M. (2013). NGA-West 2 equations for predicting PGA, PGV, and 5%-Damped PSA for shallow crustal earthquakes. *Earthquake*

Spectra, **30**(3).

35. Chen, S.-Z., and Atkinson, G.M. (2002) Global comparisons of earthquake source spectra. *Bulletin of the Seismological Society of America*, **92**, 885-895.

36. Meghdadi, A. and Shoja-Taheri, J. (2014) Ground-motion attenuation and source spectral shape for earthquakes in eastern Iran. *Bulletin of the Seismological Society of America*, **104**, 624-633.

37. Boore, D.M., Di Alessandro, C., and Abrahamson, N.A. (2014) A generalization of the double-corner-frequency source spectral model and its use in the SCEC BBP Validation Exercise. *Bulletin of the Seismological Society of America*, **104**, 2387-2398.

38. Boore, D.M. (2014) Written Communication.